Tests of gravitational symmetries with pulsar binary J1713+0747

W. W. Zhu,[1,2]★ G. Desvignes,[1] N. Wex,[1]★ R. N. Caballero,[1] D. J. Champion,[1]
P. B. Demorest,[3] J. A. Ellis,[4] G. H. Janssen,[5,6] M. Kramer,[1,7] A. Krieger,[1] L. Lentati,[8]
D. J. Nice,[9] S. M. Ransom,[10] I. H. Stairs,[11] B. W. Stappers,[7] J. P. W. Verbiest,[1,12]
Z. Arzoumanian,[13,14] C. G. Bassa,[5] M. Burgay,[15] I. Cognard,[16,17] K. Crowter,[11]
T. Dolch,[18] R. D. Ferdman,[19] E. Fonseca,[20] M. E. Gonzalez,[11,21] E. Graikou,[1]
L. Guillemot,[16,17] J. W. T. Hessels,[5,22] A. Jessner,[1] G. Jones,[23] M. L. Jones,[2,24,30]
C. Jordan,[7] R. Karuppusamy,[1] M. T. Lam,[24,25] K. Lazaridis,[1] P. Lazarus,[1] K. J. Lee,[1,26]
L. Levin,[7] K. Liu,[1] A. G. Lyne,[7] J. W. McKee [ORCID],[1,7] M. A. McLaughlin,[24,25]
S. Osłowski,[1,12,27] T. Pennucci,[24,28] D. Perrodin,[15] A. Possenti,[15] S. Sanidas,[7,22]
G. Shaifullah [ORCID],[1,5,12] R. Smits,[5] K. Stovall,[3] J. Swiggum,[29] G. Theureau[16,17,30] and
C. Tiburzi [ORCID][1,12]

Affiliations are listed at the end of the paper

ABSTRACT

Symmetries play a fundamental role in modern theories of gravity. The strong equivalence principle (SEP) constitutes a collection of gravitational symmetries which are all implemented by general relativity. Alternative theories, however, are generally expected to violate some aspects of SEP. We test three aspects of SEP using observed change rates in the orbital period and eccentricity of binary pulsar J1713+0747: (1) the gravitational constant's constancy as part of locational invariance of gravitation; (2) the universality of free fall (UFF) for strongly self-gravitating bodies; (3) the post-Newtonian parameter $\hat{\alpha}_3$ in gravitational Lorentz invariance. Based on the pulsar timing result of the combined data set from the North American Nanohertz Gravitational Observatory and the European Pulsar Timing Array, we find $\dot{G}/G = (-0.1 \pm 0.9) \times 10^{-12}\,\mathrm{yr}^{-1}$, which is weaker than Solar system limits, but applies for strongly self-gravitating objects. Furthermore, we obtain an improved test for a UFF violation by a strongly self-gravitating mass falling in the gravitational field of our Galaxy, with a limit of $|\Delta| < 0.002$ (95 per cent C.L.). Finally, we derive an improved limit on the self-acceleration of a gravitationally bound rotating body, to a preferred reference frame in the Universe, with $-3 \times 10^{-20} < \hat{\alpha}_3 < 4 \times 10^{-20}$ (95 per cent C.L.). These results are based on direct UFF and $\hat{\alpha}_3$ tests using pulsar binaries, and they overcome various limitations of previous tests of this kind.

Key words: gravitation – binaries: general – stars: neutron – pulsars: individual (PSR J1713+0747).

1 INTRODUCTION

Einstein's equivalence principle (EEP) is one of the guiding ideas that aided Einstein to conceive the theory of general relativity (GR).

EEP states that non-gravitational experiments in a local Lorentz frame should give the same result regardless of when and where they take place. This principle helped in establishing the idea that gravity is the manifestation of curved spacetime, which can be abstracted as a four-dimensional manifold endowed with a Lorentzian metric, where freely falling test bodies follow geodesics of that metric (universality of free fall), and the local non-gravitational laws of physics are those of special relativity. Gravity theories built upon

this concept are called 'metric theories of gravity', like GR and scalar–tensor theories. See Will (1993) for details.

The strong equivalence principle (SEP) extends the EEP by including local gravitational aspects of the test system (Will 2014). The universality of free fall (UFF) is extended to self-gravitating bodies, which fall in an external gravitational field. Furthermore, local test experiments, including gravitational ones, should give the same results regardless of the location or velocity of the test system. It is conjectured that GR is the only gravity theory that fully embodies SEP.[1] Although in metric theories of gravity all matter fields couple only to one physical metric ('universal coupling'), alternatives to GR generally introduce auxiliary gravitational fields (e.g. one or more scalar fields) which ultimately lead to a violation of SEP at some point. For this reason, testing the symmetries related to SEP has strong potential to either exclude (or tightly constrain) alternative gravity theories or falsify GR. It is therefore a powerful tool in searching for new physics. To date, all experimental evidence supports SEP and therefore GR (Will 2014; Shao & Wex 2016).

The post-Newtonian parametrization (PPN) is a formalism introduced by Thorne & Will (1971) and Will & Nordtvedt (1972) to describe generically the potential deviation from GR in metric theories of gravitation at the post-Newtonian level. Through a set of simple assumptions, such as slow-motion, weak field, and no characteristic length scales in the gravitational interaction, the PPN formalism can encompass most metric theories using only 10 parameters. Most of these PPN parameters (or combinations of them) are directly related to a violation of specific aspects of SEP. For strongly self-gravitating bodies, like neutron stars, these PPN parameters become kind of body-dependent quantities, which are functions of the compactness of the bodies of the system (see e.g. Damour 2009). Hence, one can have situations where a theory is in (nearly) perfect agreement with GR in the Solar system, but shows significant violations of SEP in the presence of strongly self-gravitating bodies. A particularly extreme example is spontaneous scalarization, which is a non-perturbative strong-gravity effect that is known for certain scalar–tensor theories (Damour & Esposito-Farese 1993).

Alternative theories of gravity, generally, also predict a temporal change in the locally measured Newtonian gravitational constant G, which is caused by the expansion of the Universe (Will 1993; Uzan 2011). Such a change in the local gravitational constant constitutes a violation of the local position invariance, which also refers to position in time. Hence, a varying G directly violates one of the three main pillars of SEP. One of the testable consequences of a change in G are changes in the orbital parameters of the Solar system and binary systems, in particular the size of an orbit and the orbital period. Again, the situation is more complicated in the presence of strongly self-gravitating bodies (Nordtvedt 1990; Wex 2014). Specifically, most gravitational theories that violate SEP also predict the existence of dipolar gravitational radiation (DGR). The presence of DGR would be a very efficient way of draining orbital energy from a pulsar-white dwarf binary. Therefore, in a strong field test using pulsar, one often has to consider both the variation of G and the existence of DGR simultaneously as is done in this work.

Another important pillars of SEP is the extension of the UFF to objects with significant gravitational binding energy, E^{grav}, i.e. the weak equivalence principle (WEP) is valid for test particles as well as for self-gravitating bodies. Every metric theory of gravity,

by definition, fulfills WEP for test particles. On the other hand, alternatives to GR are usually expected to violate WEP in the interaction of self-gravitating bodies (Will 1993, 2014). According to such theories, objects with different binding energy feel different accelerations in an external gravitational field g. More specifically, a binary system composed of two stars with different compactness would undergo a 'gravitational Stark effect' that polarizes the binary orbit in a characteristic way. In the Earth-Moon system, this is called the Nordtvedt effect and has been tightly constrained by Lunar Laser Ranging (LLR; Nordtvedt 1968; Müller, Hofmann & Biskupek 2012; Williams, Turyshev & Boggs 2012). Pulsar binary systems falling in the gravitational field of our Galaxy would (slowly) oscillate between a more and less eccentric configuration. This makes pulsar-white dwarf binary a viable laboratory for testing strong-field UFF (Damour & Schäfer 1991).

Some alternative theories of gravity violate SEP by introducing a preferred frame of reference for the gravitational interaction. Generally, this preferred frame can be identified with the global mass distribution in the Universe, which is the frame in which the cosmic microwave background (CMB) is isotropic, i.e. has no dipole. In the PPN formalism, there are three parameters, α_1, α_2, and α_3, which are related to such kinds of symmetry breaking. The parameter α_3 is linked to two effects, a preferred frame effect and a violation of conservation of total momentum (Will 1993). In this paper, we test the PPN parameter α_3 through the fact that it causes an anomalous self-acceleration of a spinning body, which is proportional to and perpendicular to the object's spin and motion with respect to the preferred frame. Such acceleration would lead to an observable effect in a binary system, such as an anomalous drift in the eccentricity of the binary. PSR J1713+0747, due to its high spin frequency and measurable proper motion, has the best figure of merit for testing α_3 in the present. More precisely, with binary pulsars one tests the quantity $\hat{\alpha}_3$, which is a generalization of α_3 to a situation with strongly self-gravitating objects. Therefore, $\hat{\alpha}_3$ also contains preferred frame effects related to the binding energy of the neutron star (cf. discussion in Damour & Esposito-Farèse 1992b; Will 2018).

Some pulsar binary systems are particularly useful for certain tests of SEP (see Shao & Wex 2016, for a recent review). In this paper, we measure the change rate in the orbital periodicity and eccentricity of the pulsar-white dwarf binary PSR J1713+0747 and use that to test the following three aspects of SEP: (1) the gravitational constant's constancy; (2) the UFF for strongly self-gravitating bodies; (3) the PPN parameter $\hat{\alpha}_3$ in the context of Lorentz invariance of gravitation and conservation of total momentum. Section 2.1 describes the pulsar timing; Sections 2.2, 2.3, and 2.4 describe the test for the gravitational constant's constancy, the UFF test, and the test for $\hat{\alpha}_3$. In Section 3, we give the conclusion and the summary.

2 METHOD AND RESULTS

PSR J1713+0747 is a millisecond pulsar orbiting a $0.29\,\mathrm{M_{\odot}}$ white dwarf. The pulsar's short spin period (4.5 ms) and narrow pulse profile enable us to measure its pulse time of arrivals (TOAs) at sub-microsecond precision. This pulsar is monitored by the North American Nanohertz Gravitational Observatory (NANOGrav), the European Pulsar Timing Array (EPTA), and the Parkes Pulsar Timing Array for the purpose of detecting nHz gravitational waves. A major part of the data used in this work comes from the NANOGrav[2]

---

[1]There is one known exception, which however is falsified by Solar system experiments (Deruelle 2011).

[2]www.nanograv.org

and EPTA programs. The EPTA[3] is a collaboration of European institutes to work towards the direct detection of low-frequency gravitational waves and the running of the Large European Array for Pulsars. These data were taken between 1993 and 2014 using observatories including William E. Gordon Telescope of Arecibo observatory, Robert C. Byrd Green Bank Telescope, Effelsberg Telescope, Lovell Telescope of Jodrell Bank observatory, Nançay Radio Telescope, and Westerbork Synthesis Radio Telescope. Splaver et al. (2005) published the early data set for J1713+0747 from Arecibo and Green Bank Telescope (GBT). Subsequently, Zhu et al. (2015) published the combined J1713+0747 data from Splaver et al. (2005) and NANOGrav 9 yr data release (Arzoumanian et al. 2015). Desvignes et al. (2016) published the data and timing analysis for the EPTA pulsars including J1713+0747. This work presents the first timing analysis of the combined J1713+0747 data published in Zhu et al. (2015) and Desvignes et al. (2016). We are able to model very accurately the binary system's orbit through various time-delaying effects like Römer delay, Shapiro delay, and annual-orbital parallax. From these we can measure the masses of the two stars, the sky orientation and inclination angle of the orbit, and the position and proper motion of the system. The modelling was performed using the pulsar timing software TEMPO2 (Edwards, Hobbs & Manchester 2006) and the ting parameters are listed in Table 1.

2.1 Pulsar binary timing

For the timing of PSR J1713+0747, we employ an extended version of the *ELL1*[4] pulsar binary model (Lange et al. 2001), which is valid for $e \equiv |\boldsymbol{e}| \ll 1$, where $\boldsymbol{e}$ is the eccentricity vector of the orbit. *ELL1* models a pulsar binary orbit with small eccentricity by decomposing $\boldsymbol{e}$ into two orthogonal vectors e_x and e_y, where $e_x \equiv e \cos \omega$ and $e_y \equiv e \sin \omega$, and ω is the longitude of periastron, i.e. the angle between $\boldsymbol{e}$ and the ascending node. We use e_x to represent the component of $\boldsymbol{e}$ pointing from the centre of the orbit to the ascending node and e_y represents the part pointing from Earth to the pulsar. Lange et al. (2001) showed that the Römer delay of a small eccentricity orbit can be expressed simply as $\Delta_R = x[\sin \phi + (e_y/2)\sin 2\phi - (e_x/2)\cos 2\phi]$, omitting higher order terms proportional to $\mathcal{O}(xe^2)$. Here x is the projected semimajor axis of the pulsar orbit in units of light seconds, and $\phi \equiv n_b(T - T_{asc})$, where $n_b = 2\pi/P_b$ is the orbital frequency, T the time of the pulsar, and T_{asc} the so-called time of the ascending node (see Lange et al. 2001 for details). However, we find that the precision of this expression is insufficient for modelling PSR J1713+0747's Römer delay due to its timing precision. To increase the precision of our timing model, we extend the *ELL1* model by including the second-order terms:

$$\Delta_R = x\left(\sin \phi - \frac{e_x}{2}\cos 2\phi + \frac{e_y}{2}\sin 2\phi\right)$$
$$- \frac{x}{8}\left(5e_x^2 \sin \phi - 3e_x^2 \sin 3\phi - 2e_x e_y \cos \phi\right.$$
$$\left. + 6e_x e_y \cos 3\phi + 3e_y^2 \sin \phi + 3e_y^2 \sin 3\phi\right) + \mathcal{O}(xe^3). \quad (1)$$

This extended *ELL1* model (*ELL1* +) is sufficient for modeling PSR J1713+0747 since its $xe^3 \sim 0.01$ ns. Furthermore, we express $\boldsymbol{e}$ as a function of time $[e_x(t) = e_x(t_0) + \dot{e}_x t$ and $e_y(t) = e_y(t_0) + \dot{e}_y t]$ to model the effect of a changing eccentricity, where $\dot{e}_x$ and $\dot{e}_y$ represent the change rate of $\boldsymbol{e}$ in time. The higher order terms of

equation (1) could then straightforwardly be added to the existing implementation of the *ELL1* model in TEMPO2 (Edwards et al. 2006).

Apart from the changes in the binary model, the rest of the timing analysis follows those in Zhu et al. (2015) and Desvignes et al. (2016). For a high-timing precision pulsar such as PSR J1713+0747, it is necessary to employ a comprehensive noise model including dispersion measure (DM) variation, jitter noise, and red noise.

For example, the latest Arecibo 1400 MHz and 2300 MHz band observations have 800 MHz bandwidth broken into multiple subbands. A single wideband observation like this is already constraining DM very well. Additionally, in every NANOGrav observing

Table 1. Timing model parameters[a] from TEMPO2.

Parameter	Best-fitting values
Measured parameters	
Right ascension, α (J2000)	17:13:49.5320247(9)
Declination, δ (J2000)	7:47:37.50612(2)
Proper motion in α, $\mu_\alpha = \dot{\alpha}\cos\delta$ (mas yr^{-1})	4.918(3)
Proper motion in δ, $\mu_\delta = \dot{\delta}$ (mas yr^{-1})	$-3.915(5)$
Parallax, π (mas)	0.87(4)
Spin frequency, ν (s^{-1})	218.8118438547250(3)
Spin down rate, $\dot{\nu}$ (s^{-2})	$-4.08379(4) \times 10^{-16}$
Dispersion measure[b] (pc cm^{-3})	15.970
Orbital period, P_b (d)	67.8251299228(5)[c]
Change rate of P_b, $\dot{P}_b$ (10^{-12} s s^{-1})	0.34(15)
$\hat{x}$ component of the eccentricity, e_x	$-0.0000747752(7)$
$\hat{y}$ component of the eccentricity, e_y	0.0000049721(19)
Change rate of e_x, $\dot{e}_x$ (s^{-1})	$0.4(4) \times 10^{-17}$
Change rate of e_y, $\dot{e}_y$ (s^{-1})	$-1.7(4) \times 10^{-17}$
Time of ascending node, T_{asc} (MJD)	53727.836759558(6)
Projected semimajor axis, x (lt-s)	32.34242184(12)
Orbital inclination, i (deg)	71.69(19)
Companion mass, $M_c/M_\odot$	0.290(11)
Position angle of ascending node, Ω (deg)	89.7(6)
Profile frequency dependency parameter, FD1[d]	$-0.00016376(18)$
Profile frequency dependency parameter, FD2[d]	0.0001363(3)
Profile frequency dependency parameter, FD3[d]	$-0.0000672(6)$
Profile frequency dependency parameter, FD4[d]	0.0000152(5)
Fixed parameters	
Solar system ephemeris	DE421
Reference epoch for α, δ, and ν (MJD)	53729
Red noise amplitude	-13.451
Red noise spectral index	-1.867
Derived parameters	
Intrinsic period derivative, $\dot{P}_{Int}$ (s s^{-1})	$8.96(3) \times 10^{-21}$
Pulsar mass, $M_p/M_\odot$	1.33(10)
Dipole magnetic field, B (G)	$2.048(3) \times 10^{8}$
Characteristic age, τ_c (yr)	$8.08(3) \times 10^{9}$

Notes. [a]We extend TEMPO2's *T2* binary model to include higher order corrections from the *ELL1* model. The numbers in parentheses indicate the uncertainties on the last digit(s). Uncertainties on parameters are estimated from the result of MCMC$n_b = 2\pi/P_b$ process in which the timing and noise model were evaluated.
[b]The averaged DM value based on the DMX model.
[c]Most pulsar timing model parameters presented in this paper are consistent with those reported in Zhu et al. (2015) except for the orbital period P_b. This is because P_b is defined differently in *ELL1* model used here from the *DD* model used in Zhu et al. (2015). In *DD* model, P_b is defined as the time between two periastron passings, while in *ELL1* model, P_b is the time between two ascending node passings.
[d] See Zhu et al. (2015) and Arzoumanian et al. (2015) for the description and discussion of the FD model.

---

[4]The name ELL1 comes from the fact that eccentricity (e) is much less (LL: less less) than one (1).

session, we often observe a pulsar using a high-frequency receiver and a low-frequency receiver 'back-to-back' in less than two days. These two observations when combined offer even wider effective bandwidth than a single receiver observation. This observing scheme would enable us to very precisely measure DM in the two days where multiband observations happened but does not constrain the pulsar's DM for the days between the observations as precisely. For this reason, the DMX model is well suited for fitting NANOGrav data and is agnostic to sudden changes in dispersion as observed in the 2008 J1713+0747 data (Zhu et al. 2015; Desvignes et al. 2016). In contrast, the EPTA TOAs typically have a slightly smaller bandwidth and are often not grouped into tight sessions, but there are many EPTA observations forming a slightly higher observation cadence than NANOGrav observations. These TOAs are better modelled using a continuous power-law Gaussian process model plus a special DM event model to fit both the slow changes in dispersion and the aforementioned sudden non-Gaussian dispersion changes.

In this work, we use two different approaches to model the DM variation. The first one is based on the noise analysis technique described in van Haasteren & Levin (2013), Ellis (2013), Dolch et al. (2014), Zhu et al. (2015), Arzoumanian et al. (2015), and Dolch et al. (2016). In this approach, we use the *DMX* model that groups TOAs into epochs and fit one DM value for each epoch. We use a dynamic scheme to group TOAs: we put the Arecibo/GBT wideband TOAs into small groups and attach to them any TOAs within five days. We then group the rest of TOAs, including most EPTA TOAs and early-day NANOGrav TOAs, into DMX bins spanning less than 11 d. This scheme allows us to put all TOAs into small groups and fit each group with one DM value, respectively. We model jitter noise as correlated noises between TOAs from the same observations and the red noise as a stationary Gaussian process with a power-law spectrum. This analysis is conducted using the PAL2 software package[5] (Ellis & van Haasteren 2017). The second approach models DM variation as a power-law Gaussian process (Lentati et al. 2013) with 21 coefficients plus a special DM event model to fit the 2008 'dipping' of J1713+0747's DM. This analysis is conducted using the TEMPONEST[6] software package (Lentati et al. 2014). Despite the different ways of treating DM variations, we find completely consistent results in the best-fitting timing and noise model from both approaches, with the second approach yielding slightly smaller parameter uncertainties. Since we are mostly interested in testing theories of gravitation, we choose to base our tests on the result from the first approach (presented in Table 1) because it yields slightly more conservative uncertainty on $\dot{e}$. The new timing solutions based on the *ELL1* model and the combined data set are also in good agreement with the previous solutions from fitting *DD* model to NANOGrav-only data set (Zhu et al. 2015) and EPTA-only data set (Desvignes et al. 2016).

We use the Solar system ephemeris DE421 (Folkner, Williams & Boggs 2009) in the timing analysis instead of the more recent DE436 (Folkner & Park 2016). Arzoumanian et al. (2018) showed that using DE436 leads to some marginally different timing results from using DE421. The discrepancies in different Solar system ephemerides are in the masses and orbits of the outer Solar system bodies; they cause extra timing residuals in time-scales of the orbital periods of these bodies. PSR J1713+0747's orbital period is substantially smaller than those Solar system bodies. Therefore, different Solar
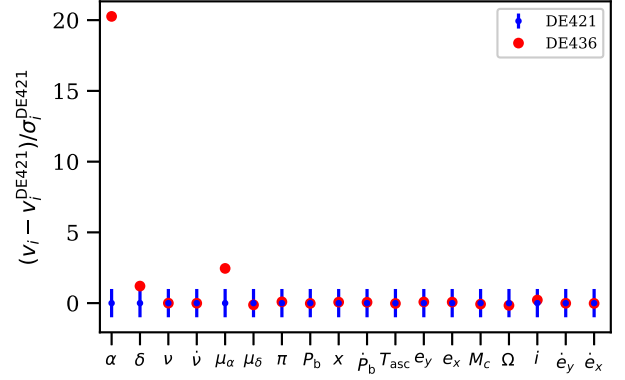
Figure 1. A comparison between DE436 and DE421 timing solution when fitting a simulated data set. The plot shows $(v_i - v_i^{\mathrm{DE421}})/\sigma_i^{\mathrm{DE421}}$, where v_i is the value of parameter i and σ_i is the uncertainty of parameter i from Table 1. The blue error bars indicate the DE421-based timing parameters with their uncertainties scaled to unity, while the red dots are the DE436-based parameters we get from fitting the simulated data set.

Table 2. Parameters changed for $>3\sigma$ when switching from DE421 to DE436 based on our simulated data set.

Parameter	DE421	DE436
Right ascension, α (J2000)	17:13:49.5320247(9)	17:13:49.5320424

system ephemerides would only marginally impact on our primary parameters of interest: $\dot{P}_{\mathrm{b}}$ and $\dot{e}$.

To evaluate Solar system ephemerides' impact on our timing solution, we use TEMPO2 to generate a synthetic data set following our DE421 solution in Table 1. We then fit the data set using DE436 to see if any timing parameters would change significantly. Indeed, we find that astrometry parameters such as position and proper motion of the system to change, but orbital parameters such as $\dot{P}_{\mathrm{b}}$ and $\dot{e}$ are not affected. Fig. 1 shows a comparison between the DE421 parameters and the DE436 parameters based on the same simulated data set and Table 2 lists the astrometry parameter that varied significantly.

2.2 Testing the time variation of *G*

Through pulsar timing, we measure the apparent change rate of the binary's orbital period ($\dot{P}_{\mathrm{b}} = (0.34 \pm 0.15) \times 10^{-12}$ s s^{-1}, Table 1). Despite being not statistically significant, the observed $\dot{P}_{\mathrm{b}}$ is consistent with what one expects from the apparent orbital period change caused by the binary's transverse motion (a.k.a. Shklovskii effect; Shklovskii 1970) and line-of-sight acceleration:

$$\dot{P}_{\mathrm{b}}^{\mathrm{Shk}} = (\mu_\alpha^2 + \mu_\delta^2)\frac{d}{c}P_{\mathrm{b}} = (0.65 \pm 0.03) \times 10^{-12} \text{ s s}^{-1}, \qquad (2)$$

$$\dot{P}_{\mathrm{b}}^{\mathrm{Gal}} = \frac{A_G}{c}P_{\mathrm{b}} = (-0.34 \pm 0.02) \times 10^{-12} \text{ s s}^{-1}. \qquad (3)$$

Here, μ_α and μ_δ are the proper motion in right ascension and declination, respectively, d is the distance from timing parallax, c is the speed of light, and A_G is the system's line-of-sight acceleration computed using the Galactic potential in McMillan (2017) (see discussion in Appendix). Subtracting these two (external) contributions from the observed $\dot{P}_{\mathrm{b}}^{\mathrm{Obs}}$ yields the residual change rate of the

orbital period

$$\dot{P}_{\rm b}^{\rm Res} = \dot{P}_{\rm b}^{\rm Obs} - \dot{P}_{\rm b}^{\rm Shk} - \dot{P}_{\rm b}^{\rm Gal} = (0.03 \pm 0.15) \times 10^{-12}\,{\rm s\,s}^{-1}, \quad (4)$$

which is consistent with the much smaller and undetectable intrinsic change $\dot{P}_{\rm b}^{\rm GR} = -6 \times 10^{-18}\,{\rm s\,s}^{-1}$ from quadrupolar gravitational radiation as predicted by GR.

This apparent consistency allows us to test the change rate of the (local) gravitational constant ($\dot{G}$) over the time span of the observation, since a $\dot{G}$ could lead to an observable change in $P_{\rm b}$ (Damour, Gibbons & Taylor 1988), which has already been used to constrain $\dot{G}$ with binary pulsars (Damour et al. 1988; Kaspi, Taylor & Ryba 1994; Nice et al. 2005; Verbiest et al. 2008; Deller et al. 2008; Lazaridis et al. 2009; Freire et al. 2012; Zhu et al. 2015).

Nordtvedt (1990) pointed out that a change of the gravitational constant also leads to changes in the neutron star's compactness and mass, and consequently leads to an additional contribution to $\dot{P}_{\rm b}$ which needs to be incorporated in our $\dot{G}$ tests with binary pulsars. If the companion is a weakly self-gravitating body, like in the case of PSR J1713+0747, then one finds to leading order (cf. equation 18 in Nordtvedt 1990)

$$\dot{P}_{\rm b}^{\dot{G}} \simeq -2\frac{\dot{G}}{G}\left[1 - \frac{2M_{\rm p} + 3M_{\rm c}}{2(M_{\rm p} + M_{\rm c})}s_{\rm p} - \frac{2M_{\rm c} + 3M_{\rm p}}{2(M_{\rm p} + M_{\rm c})}s_{\rm c}\right]P_{\rm b}, \quad (5)$$

where $M_{\rm p}$ and $M_{\rm c}$ are the pulsar mass and the companion mass, respectively. The quantity $s_{\rm p}$ denotes the 'sensitivity' of the neutron star and the white dwarf and are given by (cf. Will 1993)

$$s_{\rm p} \equiv -\left.\frac{\partial \ln M_{\rm p}}{\partial \ln G}\right|_N \quad \text{and} \quad s_{\rm c} \equiv -\left.\frac{\partial \ln M_{\rm c}}{\partial \ln G}\right|_N, \quad (6)$$

respectively, where the number of baryons N is held fixed. The sensitivity $s_{\rm p}$ of a neutron star depends on its mass, its equation of state (EoS), and the theory of gravity under consideration. As a reference, for Jordan–Fierz–Brans–Dicke (JFBD) gravity and the EoS AP4 in Lattimer & Prakash (2001) one finds for a $1.33\,{\rm M}_\odot$ neutron star, like PSR J1713+0747, $s_{\rm p} \simeq 0.16$. Following Damour & Esposito-Farèse (1992a), we further assume, as a first order approximation, that $s_{\rm p}$ is proportional to the mass

$$s_{\rm p} = 0.16\left(\frac{M_{\rm p}}{1.33\,{\rm M}_\odot}\right). \quad (7)$$

We will use this (simplified) relation in our generic calculations below but will keep in mind that depending on the EoS and the theory of gravity, equation (7) might only be a rough estimate. Furthermore, it is important to note that the usage of the sensitivity (6) and equation (7) comes with certain assumptions about how gravity can deviate from GR in the strong field of neutron stars. It is evident that such a description cannot capture non-perturbative strong-field effects, like those discussed by Damour & Esposito-Farese (1993). For a weakly self-gravitating body A, one has $s_A \simeq -E_A^{\rm grav}/M_A c^2$, where $E_A^{\rm grav}$ is the gravitational binding energy of the body. Hence, one has $s_{\rm c} \simeq 3 \times 10^{-5}$ for the white dwarf companion to PSR J1713+0747 – negligible in equation (5).

A time-varying gravitational constant generally indicates a violation of SEP. On the other hand, most gravitational theories that violate SEP also predict the existence of DGR. Such waves are very efficient in draining orbital energy from a (asymmetric) binary. The gravitational wave damping due to DGR enters the equations of motion of a binary already at the 1.5 post-Newtonian (v^3/c^3) level (see e.g. Mirshekari & Will 2013), and to leading order adds the following change to the orbital period

$$\dot{P}_{\rm b}^{\rm D} \simeq -\frac{2G}{c^3}\,n_{\rm b}\,\frac{M_{\rm p}M_{\rm c}}{M_{\rm p} + M_{\rm c}}\,\kappa_{\rm D}(s_{\rm p} - s_{\rm c})^2 + \mathcal{O}(s_{\rm p}^3), \quad (8)$$
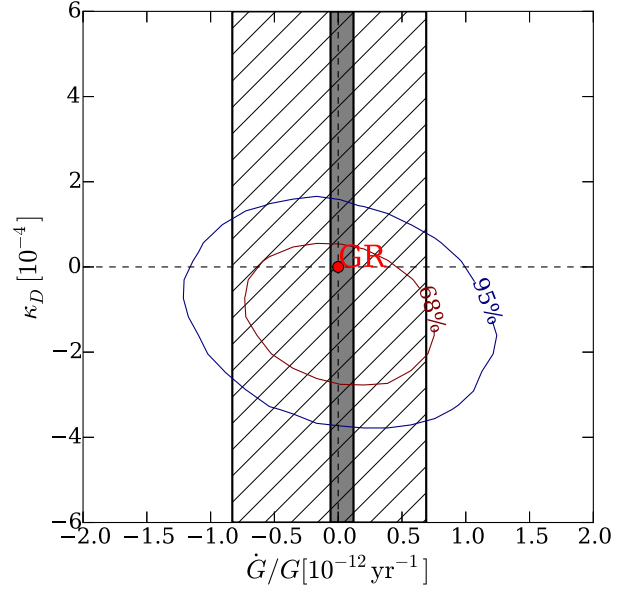

Figure 2. Confidence contours of $\dot{G}/G$ and $\kappa_{\rm D}$ computed from MCMC simulations based on timing results of PSRs J0437−4715, J1738+0333, and J1713+0747. The shaded area and grey area mark the 95 per cent confidence limit from LLR (Hofmann, Müller & Biskupek 2010) and planetary ephemerides (Fienga et al. 2015), respectively.

where $n_{\rm b} \equiv 2\pi/P_{\rm b}$ (Will 1993). The quantity $\kappa_{\rm D}$ is a body-independent constant, which depends on the fundamental parameters of the gravity theory under consideration. In JFBD gravity, for instance, one finds that

$$\kappa_{\rm D} = \frac{2}{\omega_{\rm BD} + 2}, \quad (9)$$

where $\omega_{\rm BD}$ is the Brans–Dicke parameter (Will 1993).[7] For completeness, we have kept $s_{\rm c}$ in equation (8) although, as mentioned above, it is negligible in our case.

As emphasized by Lazaridis et al. (2009), in a theory-agnostic approach the test of $\dot{G}$ and $\kappa_{\rm D}$ requires at least two pulsar binary systems with different orbital periods to break the degeneracy between the two contributions: equation (5) and equation (8). This is because the extra variation in the orbital period due to DGR is stronger in binaries with shorter orbits ($\propto P_{\rm b}^{-1}$) while that caused by $\dot{G}$ increases with orbital period ($\propto P_{\rm b}$). Therefore, testing $\dot{G}/G$ using binaries of significantly different orbital periods breaks the degeneracy between the two effects (see Lazaridis et al. 2009, for further details). Here, we adapt the method of Lazaridis et al. (2009) and incorporate results from three different pulsar-white dwarf systems, namely PSRs J0437−4715 (Reardon et al. 2016) and J1738+0333 (Freire et al. 2012), in combination with the results for PSR J1713+0747 obtained in this work. Each pulsar provides a constraint on $\dot{P}_{\rm b}^{\rm D} + \dot{P}_{\rm b}^{\dot{G}}$, and hence via equations (5) and (8) excludes certain regions in the $\dot{G}/G$–$\kappa_{\rm D}$ plane. As a result of the large difference in orbital period, these constraints are complementary and consequently lead to a small region of allowed values in the $\dot{G}/G$–$\kappa_{\rm D}$ plane (see Fig. 2). The individual constraints on $\dot{G}$ and $\kappa_{\rm D}$ are

$$\dot{G}/G = (-0.1 \pm 0.9) \times 10^{-12}\,{\rm yr}^{-1}, \quad (10)$$

---

[7]In JFBD gravity the effective scalar coupling α_A and the sensitivity s_A of a neutron star are related by $\alpha_A = \alpha_0(1 - 2s_A)$ (cf. chapter 8 in Damour & Esposito-Farèse 1992a).

$$\kappa_D = (-0.7 \pm 2.2) \times 10^{-4}\,. \tag{11}$$

They improve the Zhu et al. (2015) results based on NANOGrav-only PSR J1713+0747 data by ~20 per cent in $\dot{G}/G$ and ~30 per cent in κ_D.

2.3 Testing the universality of free fall for strongly self-gravitating bodies

Damour & Schäfer (1991) showed that, in the presence of a UFF violation, the observed eccentricity of the pulsar-white dwarf orbit could be expressed as a combination of an intrinsic eccentricity and a forced eccentricity:

$$e_F = \frac{\Delta \cdot \boldsymbol{g}_\perp c^2}{2\mathcal{F}\mathcal{G}(M_p + M_c)n_b^2}\,. \tag{12}$$

Here $\mathcal{F}$ is a theory-dependent (and 'sensitivity'-dependent) factor that accounts for potential deviations from GR in the rate of periastron advance $\dot{\omega}$. By definition, $\mathcal{F} = 1$ in GR and indeed, it is constrained to be close to one by observations. For instance, from the Double Pulsar PSR J0737−3039A/B (Burgay et al. 2003; Lyne et al. 2004) one can quite generically infer that $|\mathcal{F} - 1| \lesssim 10^{-3}$ (Kramer & Wex 2009). Therefore, we can safely assume $\mathcal{F} = 1$ in our analysis, in particular since the mass of PSR J1713+0747 is comparable to the masses in the Double Pulsar. $\mathcal{G} \approx G$ is the effective gravitational constant in the interaction between the pulsar and the white dwarf. The vector $\boldsymbol{g}_\perp$ is the projection of the Galactic acceleration $\boldsymbol{g}$ on to the orbital plane, and Δ is the fractional difference in the accelerations between the pulsar and white dwarf, and therefore a dimensionless measure of the significance of the UFF violation.

Damour & Schäfer (1991) have put forward a method to constrain Δ from small-eccentricity binary pulsars with white dwarf companions, utilizing in probabilistic considerations the smallness of the observed eccentricities. This so-called 'Damour-Schäfer' test has been extended to make use of an ensemble of suitable pulsar-white dwarf systems (Wex 1997; Stairs et al. 2005) of which the precise orbital orientations and proper motions are unknown. The currently best limits from this method are $|\Delta| < 5.6 \times 10^{-3}$ (Stairs et al. 2005) and $|\Delta| < 4.6 \times 10^{-3}$ (Gonzalez et al. 2011).[8] The validity and effectiveness of the Damour–Schäfer test rely on some (strong-field and probabilistic) assumptions. It does not improve with timing precision and is not capable of actually detecting a violation of the UFF (see discussions in Damour 2009; Freire, Kramer & Wex 2012). For this reason, it is desirable to have a direct test with a single binary pulsar. Freire et al. (2012) already identified PSR J1713+0747 as a potential candidate for such a test. In Zhu et al. (2015), PSR J1713+0747 had been used in a (single system) Damour–Schäfer test. In this work, we utilize the exquisite timing precision of PSR J1713+0747 and the tight limit on $\dot{e}$ to directly test the violation of UFF in the strong-field regime.

Based on the equation of motion, Damour & Schäfer (1991) derived that the eccentricity vector of the pulsar orbit would change
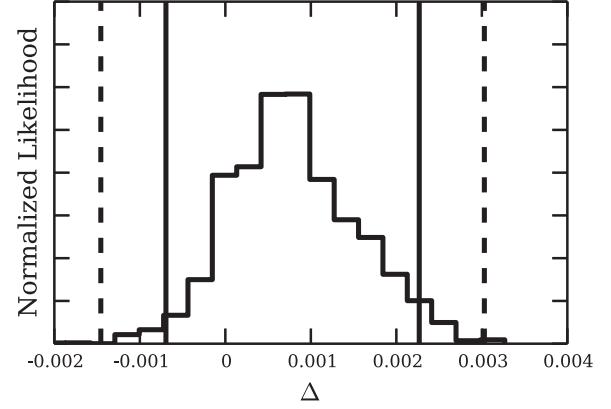
Figure 3. The normalized likelihood distribution of Δ derived from the MCMC of PSR J1713+0747's timing and noise parameters. The solid line is the 95 per cent confidence limit and dashed line marks the 99 per cent confidence limit.

according to (neglecting terms of order e^2 and smaller)

$$\dot{\boldsymbol{e}} \simeq \frac{3}{2\mathcal{V}_O} \Delta\, \boldsymbol{g} \times \hat{\boldsymbol{k}} + \dot{\omega}_{PN}\hat{\boldsymbol{k}} \times \boldsymbol{e}\,, \tag{13}$$

for given violation parameter of UFF, Δ. Here the vector $\boldsymbol{e}$ points at periastron, $\hat{\boldsymbol{k}}$ is a unit vector parallel to orbital angular momentum, $\mathcal{V}_O \equiv [\mathcal{G}(M_p + M_c)n_b]^{1/3}$ is the relative orbital velocity between the two stars. The second term describes the post-Newtonian periastron advance rate:

$$\dot{\omega}_{PN} \simeq 3\mathcal{F}(\mathcal{V}_O/c)^2 n_b + \mathcal{O}(e^2). \tag{14}$$

The extended *ELL1* timing model allows us to measure the change rate of the eccentricity vector, and we do detect an apparent $\dot{e}_y = (-1.7 \pm 0.4) \times 10^{-17}$ s^{-1} along the line of sight, likely coming from the periastron advance of the orbit. After removing the contributions of periastron advance [$\dot{e}_x^{PN} = (-0.07 \pm 0.01) \times 10^{-17}$ s^{-1}, $\dot{e}_y^{PN} = (-1.0 \pm 0.1) \times 10^{-17}$ s^{-1}] according to the measured system masses and orbital parameter (Table 1 and equation 14), the resulting excess eccentricity change rate [$\dot{e}_x^{exc} = (0.4 \pm 0.4) \times 10^{-17}$ s^{-1}, $\dot{e}_y^{exc} = (0.7 \pm 0.4) \times 10^{-17}$ s^{-1}] is consistent with zero. We perform a Monte Carlo Markov Chain (MCMC) simulation that simultaneously fits both the timing model and the dispersion, jitter and red noises, using the PAL2 software. The MCMC allows us to obtain a large sample of possible timing parameter values along with their likelihood. We then use these MCMC results to calculate the Δ needed to account for the residual $\dot{e}$ excess. Fig. 3 shows the posterior distribution of Δ. From this result we derive that $-0.0007 < \Delta < 0.0023$ with 95 per cent confidence level (C.L.). The deviation from GR is insignificant. For the ease of comparison with previous results, we also derive from the above results:

$$|\Delta| < 0.002 \quad (95 \text{ per cent C.L.})\,. \tag{15}$$

This constraint improves the previous test of UFF in gravitation using this pulsar (Gonzalez et al. 2011) by more than a factor of two. More importantly, it is a direct test and therefore, as discussed above, more robust than previous Damour–Schäfer test based limits. The limit in equation (15) provides currently the best test for the UFF of a strongly self-gravitating object falling in the gravitational field of the Galaxy. We discuss the theoretical meaning of that in Section 3, in particular in view of the much tighter UFF limit from a pulsar in a stellar triple system, which has been published recently Archibald et al. (2018).

---

[8]As discussed in detail in Wex (2014), the ~20 per cent improvement from Stairs et al. 2005's $|\Delta|$ limit by Gonzalez et al. (2011) comes with a caveat, because of the inclusion of a seemingly particularly constraining pulsar which, however, violates the necessary conditions for a Damour–Schäfer test.

2.4 Testing the Lorentz invariance and conservation of momentum in gravitation

The PPN parameters α_1, α_2, and α_3 describe different symmetry breaking effects in gravitational theories that violate local Lorentz invariance in the gravitational sector. The parameters α_1 and α_2 have already been tightly constrained through binary and isolated pulsars (Shao & Wex 2012; Shao et al. 2013). In this paper, we focus on the test of α_3, but we also account for those effects related to α_1 and α_2 which in principle could have an influence on our α_3 limits.

The parameter α_3 describes a gravitational symmetry breaking that leads to both the existence of a preferred frame and a violation of conservation of momentum (Will 1993). A non-zero α_3 would give rise to an anomalous self-acceleration for a spinning self-gravitating body that moves in the preferred reference frame. One often assumes that the universal matter distribution selects the rest frame of the CMB as the preferred frame. Following the same idea, we choose CMB frame as the preferred frame in our analysis. However, our constraint on $\hat{\alpha}_3$ should be robust for preferred frames that moves at low velocity with respect to the pulsar, and it gets stronger when the selected frame is moving very fast with respect to the pulsar. A weakly self-gravitating body with mass M, gravitational binding energy $E_{\rm grav}$, rotational frequency ν, and velocity $\boldsymbol{v}_{\rm CMB}$ in the CMB frame, would undergo acceleration induced by α_3 effects:

$$\boldsymbol{a}_{\alpha_3} = -\frac{\alpha_3}{3} \frac{E_{\rm grav}}{Mc^2} 2\pi\nu \, \hat{\boldsymbol{n}}_s \times \boldsymbol{v}_{\rm CMB} \,. \tag{16}$$

Here $\hat{\boldsymbol{n}}_s$ is a unit vector in the direction of the body's spin (Will 1993). For strongly self-gravitating bodies, following Bell & Damour (1996), we replace $E_{\rm grav}/Mc^2$ by the sensitivity of the pulsar $s_{\rm p}$.[9] Furthermore, we replace α_3 by $\hat{\alpha}_3$, where the hat symbol serves as a reminder that we are testing the (body-dependent) strong-field extension of α_3, which may be different from the weak-field α_3, but is expected to be of the same order (see Section 3 for a more detailed discussion).

Similar to the violation of UFF, the acceleration caused by $\hat{\alpha}_3$ would lead to a polarization of the orbit of a rapidly rotating pulsar (Bell & Damour 1996). For fully recycled millisecond pulsars like PSR J1713+0747, $\hat{\boldsymbol{n}}_s$ likely aligns with the orbital angular momentum. For this reason, we can set $\hat{\boldsymbol{n}}_s = \hat{\boldsymbol{k}}$ in our calculations.

Besides the influence of a non-vanishing α_3, one also needs to account for contributions of α_1 and α_2 to the orbital dynamics, since in general one cannot assume α_1 and α_2 to be zero in a theory that breaks local Lorentz invariance in the gravitational sector and gives rise to an α_3. In a near-circular binary, a non-vanishing α_2 would lead to a precession of the orbital angular momentum around the direction of $\boldsymbol{w}$, which in turn leads to a temporal change in the projected semimajor axis x (Shao & Wex 2012). On the other hand $|\alpha_2|$ is constrained by pulsar experiments to be less than about 10^{-9}, which corresponds to a change in x that is about six orders of magnitude smaller than the contribution from proper motion, which is used to determine Ω. Therefore, effects from α_2 can be safely neglected in our α_3 test.

A non-vanishing α_1 adds to the polarization of the orbit in the same way as a non-vanishing α_3, and analogous to equation (13) one finds for the change of the orbital eccentricity vector

$$\dot{\boldsymbol{e}} = \dot{\boldsymbol{e}}_{\hat{\alpha}_1} + \dot{\boldsymbol{e}}_{\hat{\alpha}_3} + \dot{\omega}_{\rm PN} \hat{\boldsymbol{k}} \times \boldsymbol{e} \,, \tag{17}$$

where

$$\dot{\boldsymbol{e}}_{\hat{\alpha}_1} \simeq \frac{\hat{\alpha}_1}{4c^2} \frac{M_{\rm p} - M_{\rm c}}{M_{\rm p} + M_{\rm c}} n_{\rm b} \mathcal{V}_O \, \boldsymbol{w}_\perp \tag{18}$$

(Damour & Esposito-Farèse 1992b) and

$$\dot{\boldsymbol{e}}_{\hat{\alpha}_3} \simeq \frac{3}{2\mathcal{V}_O} \boldsymbol{a}_{\hat{\alpha}_3} \times \hat{\boldsymbol{k}} = -\hat{\alpha}_3 \pi \frac{s_{\rm p}\nu}{\mathcal{V}_O} \boldsymbol{w}_\perp \tag{19}$$

(Bell & Damour 1996). The velocity $\boldsymbol{w}_\perp$ is the projection of the systemic CMB frame velocity into the orbital plane of the binary pulsar. To independently constrain $\hat{\alpha}_3$ from PSR J1713+0747 timing, we will include the $\hat{\alpha}_1$ limits obtained from PSR J1738+0333 by Shao & Wex (2012) in our analysis. Conversely, owing to its small orbital period, PSR J1738+0333's possible $\hat{\alpha}_3$ effects would be much smaller than its $\hat{\alpha}_1$ effects and would have insignificant impact on the $\hat{\alpha}_1$ limits derived from this system. There is one assumption, however, that we have to make here. Since PSR J1713+0747 and PSR J1738+0333 have different masses, and therefore different sensitivities $s_{\rm p}$, we cannot assume that they would lead to identical $\hat{\alpha}_1$. For this reason, our analysis only applies to deviations from GR which exhibit only a moderate mass dependence of the strong-field parameter $\hat{\alpha}_1$, at least for neutron stars in the range of 1.3–1.5 $M_\odot$.

All parameters involved in the evaluation of $\dot{\boldsymbol{e}}$ are measurable through the timing of PSR J1713+0747 (Table 1), except for the radial velocity of the pulsar binary with respect to the Solar system v_r. To calculate $\dot{\boldsymbol{e}}$ from equation (17) one needs the system's three-dimensional velocity $\boldsymbol{v}_{\rm CMB}$ in the CMB rest frame. $\boldsymbol{v}_{\rm CMB}$ can in principle be computed from the binary's three-dimensional velocity $\mathbf{v}$ about our Solar system by adding the Solar system speed in the CMB rest frame, which is well known from the measurement of the CMB dipole (see Aghanim et al. 2014, for the latest measurement). We measure the pulsar's proper motion and distance (Table 1), which allows us to determine the transverse component of $\mathbf{v}$. The white dwarf companion of PSR J1713+0747 is relatively faint (Lundgren, Foster & Camilo 1996), and a measurement of the radial velocity v_r through optical spectroscopy is currently not available. Therefore, we treat v_r as a free parameter and calculate the limits on $\hat{\alpha}_3$ as a function of v_r. A limit for v_r comes from the plausible assumption that the PSR J1713+0747 system is bound to the Galaxy and therefore must be slower than the Galactic escape velocity. Taking the Galactic potential of McMillan (2017), we find v_r to be within the range of about -680 to $+460$ km s^{-1}.[10] As shown in Fig. 4, the constraint on $\hat{\alpha}_3$ tightens as $|v_r|$ gets larger because large v_r lead to large $\boldsymbol{v}_{\rm CMB}$, which enhance the polarization effects. We find the most conservative bounds for $\hat{\alpha}_3$ from the minimum value on left side of the 95 per cent C.L. contour and the maximum value of the right side of the contour, despite the fact that the two values correspond to different values of v_r:

$$-3 \times 10^{-20} < \hat{\alpha}_3 < 4 \times 10^{-20} \quad (\text{95 per cent C.L.}) \,. \tag{20}$$

This result is better than the previous best constraint on $\hat{\alpha}_3$, $|\hat{\alpha}_3| < 5.5 \times 10^{-20}$ from (Gonzalez et al. 2011), which is based on a Damour–Schäfer type of test using an ensemble of pulsars.

In this section, we present our direct $\hat{\alpha}_3$ test as a stand-alone test independent of the previous tests. However, both our UFF and $\hat{\alpha}_3$ tests rely on the measurement of $\dot{\boldsymbol{e}}$. For that reason, there is a correlation between Δ and $\hat{\alpha}_3$, and in principle there is even the possibility that they cancel each other, although this would require

---

[9]Bell & Damour (1996) introduced the compactness $c_{\rm p} = 2s_{\rm p}$.

[10]As a cross-check we also used the potential by Kenyon et al. (2008), which gives very similar results.
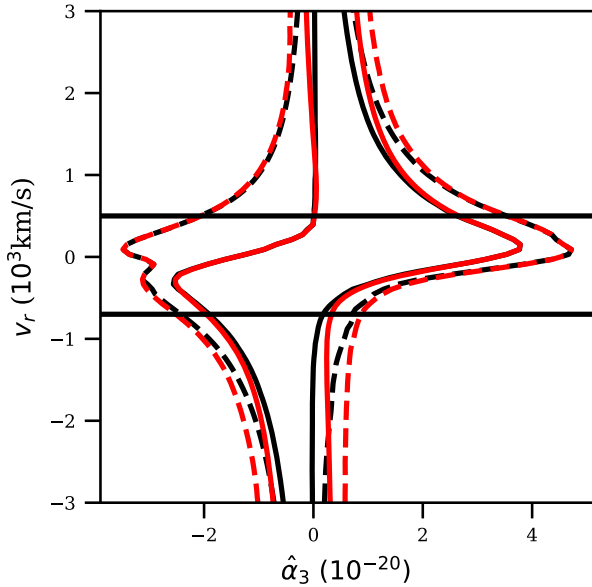
Figure 4. The likelihood distribution of $\hat{\alpha}_3$ derived from the MCMC of PSR J1713+0747's timing and noise parameters as a function of the assumed line-of-sight velocity v_r. The black solid curves corresponds to the 95 per cent C.L. and the black dashed line to the 99 per cent C.L. The red curves show the same limits with $\hat{\alpha}_1$ taken into account (see Section 2.4 for details). The two horizontal lines label the escape velocity of the pulsar binary.

rather unrealistically large v_r due to the geometrical orientation of the system. Nevertheless, our $\hat{\alpha}_3$ limit given above could be slightly optimistic. However, the recent strong-field UFF test from Archibald et al. (2018), for a more massive pulsar, have pushed Δ to ~3 orders of magnitude better than constrained in this paper (Section 2.3). When taking Archibald et al. 2018's UFF test into account, our $\hat{\alpha}_3$ limit is still valid and unaffected by the degeneracy between the two tests.

3 DISCUSSION

In this paper, we present new tests of the constancy of G, and the violations of UFF, Lorentz invariance, and conservation of momentum in gravitation. These violations of gravitational symmetries lead to changes in the orbital period and eccentricity particularly in binaries such as pulsar–white dwarf systems like J1713+0747. We conduct these tests through the measurement of an excess change in the orbital period and eccentricity from the timing analysis of PSR J1713+0747.

We repeat the combined $\dot{G}/G$, κ_D test presented in Zhu et al. (2015) by incorporating more PSR J1713+0747 timing data from EPTA and find that the result improves [$\dot{G}/G = (-0.1 \pm 0.9) \times 10^{-12}$ yr^{-1} and $\kappa_D = (-0.7 \pm 2.2) \times 10^{-4}$]. The improvement on $\dot{G}/G$ could be attributed to the inclusion of EPTA data which increased the number of TOAs used in the experiment, whereas the changes in κ_D limits are mostly due to the change from using a fiducial sensitivity function that scales linearly with neutron star mass to using a more realistic non-linear neutron star sensitivity function. Our κ_D test is a generic test of DGR, included for the purpose of generalizing the $\dot{G}/G$ test for general SEP-violating theories. More stringent tests of the DGR effects could be done with pulsar timing if one takes into account the nature of the SEP-violating theories (Freire et al. 2012). In some theories, $\mathcal{O}(s_p^3)$ terms cannot

be neglected (cf. equation 8) even in a first-order estimation. In some theory-specific tests, a more stringent limit on κ_D could come from non-radiative tests, for instance from the Solar system measurements based on the Cassini experiment, like for JFBD gravity where Cassini implies $|\kappa_D| \lesssim 9 \times 10^{-5}$ with 95 per cent confidence (cf. equation 9).

When compared directly to the Solar system tests (LLR, Hofmann et al. 2010) and planetary ephemerides (Fienga et al. 2015, Fig. 2), our $\dot{G}/G$ constraint is not as constraining. But the pulsar binary tests involve objects of much stronger self-gravitation than objects in the Solar system. The pulsar timing limits of $\dot{G}/G$ and κ_D are testing SEP-violating effects beyond linear extrapolations from the weak-field limit. Wex (2014) demonstrated that in certain theories of gravitation, $\dot{G}/G$ effects could be greatly enhanced by a strongly self-gravitating body while remaining insignificant in the Solar system.

Previous pulsar UFF tests, such as Wex (1997), Stairs et al. (2005), and Gonzalez et al. (2011) employed the idea of Damour & Schäfer (1991), which uses an ensemble of wide-orbit small-eccentricity pulsar–white dwarf binaries. The approach's effectiveness relies on the how close the orbits to being circular. And the approach's validity relies on the statistical argument that the unknown orbital orientations of a collection of pulsars are randomly and uniformly distributed. Hence the Damour & Schäfer (1991) tests cannot directly detect SEP violation and may only improve when a new pulsar binary with a better figure of merit is found. There comes a further caveat with previous tests, as these tests are based on an ensemble of systems with different neutron star masses. Hence, for this mix of neutron star masses a priori assumptions about the strong-field behaviour of gravity had to be made (Damour 2009). For our tests this is not the case, since these tests are based on a single neutron star with well-determined mass.

Damour & Schäfer (1991) also pointed out the possibility of directly testing UFF violations by constraining temporal changes in the orbital eccentricity. Such a test has the advantage of not depending on a group of pulsar binaries, the smallness of their e and assumptions on their orbital orientations. The effectiveness of this test improves with timing precision. Freire et al. (2012) identified PSR J1713+0747 as one of the best candidates for such a direct test. But at that time $\dot{e}$ was not directly modelled in the timing of that pulsar, and Freire et al. (2012) used an estimate of the upper limit of $\dot{e}$ based on the uncertainties of the measured e. As a result, Freire et al. (2012) could put some preliminary limits on UFF violations. In this paper, we conduct the first direct UFF test using a measured $\dot{e}$, which in principle could detect a violation of UFF, should the effect be strong enough.

Using an extended version of the *ELL1* timing model of Lange et al. (2001) in our analysis, we find $\dot{e} \simeq (0.4 \pm 0.4, -1.7 \pm 0.4) \times 10^{-17}$ s^{-1} (see Table 1), which is consistent with being caused by post-Newtonian periastron advance predicted by GR. We find no evidence for a violation of UFF with $|\Delta| < 0.002$, a result that improves by more than a factor of 2 from the previous constraint (Stairs et al. 2005; Gonzalez et al. 2011) based on this pulsar system. Similarly, we find $-3 \times 10^{-20} < \hat{\alpha}_3 < 4 \times 10^{-20}$, which is also better than the previous best result. These limits go beyond the PPN framework since they also capture strong-field deviations. To illustrate this, for example for α_3, we expand $\hat{\alpha}_3$ with respect to the sensitivity

$$\hat{\alpha}_3 = \alpha_3 + \alpha_3^{(1)} s_p + \alpha_3^{(2)} s_p^2 + \cdots, \tag{21}$$

then the limit in equation (20) not only constrains the weak-field counterpart, α_3, at the level of $\mathcal{O}(10^{-20})$, but also poses strong con-

straints on higher order terms, $\alpha_3^{(1)}$, $\alpha_3^{(2)}$, and so on. The same applies for the strong-field generalization of the Nordtvedt parameter that is given by $\Delta \equiv \hat{\eta}_N s_p$. Detailed accurate mapping of strong-field generalization and weak-field counterpart needs explicit calculations in specified gravity theories. Note that equations like (21) ultimately fail to capture non-perturbative strong-field deviations, like spontaneous scalarization (Damour & Esposito-Farese 1993).

The recently discovered pulsar triple system J0337+1715 (Ransom et al. 2014) is a superior laboratory for testing UFF than PSR J1713+0747 because the pulsar and its inner companion are subjected to much higher gravitational accelerations from the outer companion star. Simulations suggest improvement by at least three orders of magnitude (Berti et al. 2015; Shao 2016; Kramer 2016). Indeed, Archibald et al. (2018) timed the J0337+1775 over six years and achieved a strong field constraint on UFF of $|\Delta| < 2.6 \times 10^{-6}$. However, PSR J1713+0747 will remain to be one of the best systems for testing $\dot{G}$ with pulsars, due to its wide orbit and high timing precision, and for testing $\hat{\alpha}_3$ because of the fast rotation of this pulsar and its well-constrained orbit.

Shao, Wex & Kramer (2018) explored using pulsar binaries to limit the UFF violations towards dark matter in the Galaxy. Their results show that pulsar binaries are promising laboratories for such test that would probe whether gravity is the only interaction between normal matter and dark matter. For such kind of test, the Δ obtained from PSR J1713+0747 currently provides the best test for the UFF of a strongly self-gravitating object with respect to dark matter. We would like to emphasize that the triple system pulsar J0337+1715 does not provide any constraints here, as its limit applies only for the UFF towards ordinary matter, i.e. the outer white dwarf.

Finally, the first direct detection of gravitational waves by LIGO opened up the possibility to test gravity in the dynamical strong-field regime (Abbott et al. 2016). This promises qualitatively new tests of GR and its alternatives, complementary to tests obtained from binary pulsars (Berti et al. 2015; Will 2018). Concerning the effects tested here, they become particularly prominent in wide systems. Hence, LIGO/Virgo observations are much less constraining. For instance, the $\dot{G}$ limit obtained from the binary black hole merger GW151226 (Yunes, Yagi & Pretorius 2016) is about 17 orders of magnitude weaker than the limit presented here. It is important to note that tests with neutron stars and tests with black holes are qualitatively different. For instance, in the presence of a no-hair theorem black holes are expected to behave according to GR while the dynamics of neutron stars might be very different (cf. Damour & Esposito-Farèse 1992a).

REFERENCES

Abbott B. P. et al., 2016, Phys. Rev. Lett., 116, 221101
Aghanim N. et al., 2014, A&A, 571, A27
Archibald A. M. et al., 2018, Nature, 559, 73
Arzoumanian Z. et al., 2015, ApJ, 813, 65
Arzoumanian Z. et al., 2018, ApJS, 235, 37
Bell J. F., Damour T., 1996, Class. Quantum Gravity, 13, 3121
Berti E. et al., 2015, Class. Quantum Gravity, 32, 243001
Binney J., Tremaine S., 2008, Galactic Dynamics , 2nd edn. Princeton Univ. Press, Princeton
Burgay M. et al., 2003, Nature, 426, 531
Damour T., 2009, in Colpi M., Casella P., Gorini V., Moschella U., Possenti A., eds, Astrophysics and Space Science Library, Vol. 359, Physics of Relativistic Objects in Compact Binaries: From Birth to Coalescence. Springer-Verlag, Berlin, p. 1
Damour T., Esposito-Farèse G., 1992a, Class. Quantum Gravity, 9, 2093
Damour T., Esposito-Farèse G., 1992b, Phys. Rev., 46, 4128
Damour T., Esposito-Farese G., 1993, Phys. Rev. Lett., 70, 2220
Damour T., Schäfer G., 1991, Phys. Rev. Lett., 66, 2549
Damour T., Taylor J. H., 1991, ApJ, 366, 501
Damour T., Gibbons G. W., Taylor J. H., 1988, Phys. Rev. Lett., 61, 1151
Dehnen W., Binney J., 1998, MNRAS, 294, 429
Deller A. T., Verbiest J. P. W., Tingay S. J., Bailes M., 2008, ApJ, 685, L67
Deruelle N., 2011, Gen. Relativ. Gravit., 43, 3337
Desvignes G. et al., 2016, MNRAS, 458, 3341
Dolch T. et al., 2014, ApJ, 794, 21
Dolch T. et al., 2016, J. Phys. Conf. Ser. , 716, 012014

Edwards R. T., Hobbs G. B., Manchester R. N., 2006, MNRAS, 372, 1549
Ellis J. A.,van Haasteren R., 2017, jellis18/PAL2:PAL2, zenodo
Ellis J. A., 2013, Class. Quantum Gravity, 30, 224004
Fienga A., Laskar J., Exertier P., Manche H., Gastineau M., 2015, Celest. Mech. Dyn. Astron., 123, 325
Folkner W. M., Park R. S., 2016, Tech. rep., Jet Propulsion Laboratory, Pasadena, CA
Folkner W. M., Williams J. G., Boggs D. H., 2009, Interplanet. Netw. Prog. Rep., 178, C1
Freire P. C. C. et al., 2012, MNRAS, 423, 3328
Freire P. C. C., Kramer M., Wex N., 2012, Class. Quantum Gravity, 29, 184007
Gonzalez M. E. et al., 2011, ApJ, 743, 102
Hofmann F., Müller J., Biskupek L., 2010, A&A, 522, L5
Holmberg J., Flynn C., 2004, MNRAS, 352, 440
Kaspi V. M., Taylor J. H., Ryba M., 1994, ApJ, 428, 713
Kenyon S. J., Bromley B. C., Geller M. J., Brown W. R., 2008, ApJ, 680, 312
Kramer M., 2016, Int. J. Mod. Phys., 25, 1630029
Kramer M., Stappers B., 2015, Advancing Astrophysics with the Square Kilometre Array (AASKA14), 36
Kramer M., Wex N., 2009, Class. Quantum Gravity, 26, 073001
Kuijken K., Gilmore G., 1991, ApJ, 367, L9
Lange C., Camilo F., Wex N., Kramer M., Backer D., Lyne A., Doroshenko O., 2001, MNRAS, 326, 274
Lattimer J. M., Prakash M., 2001, ApJ, 550, 426
Lazaridis K. et al., 2009, MNRAS, 400, 805
Lentati L., Alexander P., Hobson M. P., Taylor S., Gair J., Balan S. T., van Haasteren R., 2013, Phys. Rev., 87, 104021
Lentati L., Alexander P., Hobson M. P., Feroz F., van Haasteren R., Lee K. J., Shannon R. M., 2014, MNRAS, 437, 3004
Li D., Pan Z., 2016, Radio Science, 51, 1060
Lundgren S. C., Foster R. S., Camilo F., 1996, in Johnston S., Walker M. A., Bailes M., eds, ASP Conf. Ser., Vol. 105, Pulsars: Problems and Progress, IAU Colloquium 160. Astron. Soc. Pac., San Francisco, p. 497
Lyne A. G. et al., 2004, Science, 303, 1153
McMillan P. J., 2017, MNRAS, 465, 76
Mirshekari S., Will C. M., 2013, Phys. Rev., 87, 084070
Müller J., Hofmann F., Biskupek L., 2012, Class. Quantum Gravity, 29, 184006
Nan R. et al., 2011, Int. J. Mod. Phys., 20, 989
Nice D. J., Taylor J. H., 1995, ApJ, 441, 429
Nice D. J., Splaver E. M., Stairs I. H., Löhmer O., Jessner A., Kramer M., Cordes J. M., 2005, ApJ, 634, 1242
Nordtvedt K., 1968, Phys. Rev., 170, 1186
Nordtvedt K., 1990, Phys. Rev. Lett., 65, 953
Piffl T. et al., 2014, MNRAS, 445, 3133
Prusti T. et al., 2016, A&A, 595, A1
Ransom S. M. et al., 2014, Nature, 505, 520
Reardon D. J. et al., 2016, MNRAS, 455, 1751
Reid M. J. et al., 2014, ApJ, 783, 130
Shao L., 2016, Phys. Rev. D, 93, 084023
Shao L., Wex N., 2012, Class. Quantum Gravity, 29, 215018
Shao L., Wex N., 2016, Sci. China Phys., Mech. Astron., 59, 87
Shao L., Caballero R. N., Kramer M., Wex N., Champion D. J., Jessner A., 2013, Class. Quantum Gravity, 30, 165019
Shao L., Wex N., Kramer M., 2018, Phys. Rev. Lett., 120, 241104
Shklovskii I. S., 1970, Sov. Astron., 13, 562
Splaver E. M., Nice D. J., Stairs I. H., Lommen A. N., Backer D. C., 2005, ApJ, 620, 405
Stairs I. H. et al., 2005, ApJ, 632, 1060
Thorne K. S., Will C. M., 1971, ApJ, 163, 595
Uzan J.-P., 2011, Living Rev. Relativ., 14, 2
van Haasteren R., Levin Y., 2013, MNRAS, 428, 1147
Verbiest J. P. W. et al., 2008, ApJ, 679, 675
Wex N., 1997, A&A, 317, 976
Wex N., , 2014, in Kopeikein S. M., ed., Frontiers in relativistic celestial mechanics , Vol. 2, de Gruyter, Berlin

Williams J. G., Turyshev S. G., Boggs D. H., 2012, Class. Quantum Gravity, 29, 184004
Will C. M., 1993, Theory and Experiment in Gravitational Physics. Cambridge University Press, Cambridge
Will C. M., 2014, Living Rev. Relativ., 17, 4
Will C. M., 2018, Class. Quantum Gravity, 35, 085001
Will C. M., Nordtvedt K. J., 1972, ApJ, 177, 757
Yunes N., Yagi K., Pretorius F., 2016, Phys. Rev., 94, 084002
Zhu W. W. et al., 2015, ApJ, 809, 41

APPENDIX : GALACTIC CORRECTIONS

In Section 2.2, we discuss how the changing Doppler effect related to the systemic motion of a binary pulsar causes apparent variations in the orbital parameters. An important part of the changing Doppler effect comes from the Galactic contribution to the line-of-sight acceleration between the pulsar binary and the Solar system. There are two orthogonal components in this Galactic contribution: the difference in the centrifugal acceleration in our circular motion around the Galactic centre, and the difference in the vertical acceleration caused mainly by the Galactic disc. We can derive the expected $\dot{P}_b^{Gal}/P_b$ based on our knowledge of the Galactic rotation curve and the local surface density of the Galactic disc.

Based on Damour & Taylor (1991), Nice & Taylor (1995) derived an analytical formula for calculating the apparent orbital variation using a flat rotation curve and the vertical acceleration model for the Solar vicinity. The subsequent pulsar timing works (Deller et al. 2008; Verbiest et al. 2008; Lazaridis et al. 2009; Freire et al. 2012; Zhu et al. 2015) used the same formula with the most recent Galactic disc model coming from Holmberg & Flynn (2004) and Reid et al. (2014). However, the analytical approach put forward by Damour & Taylor (1991) and Nice & Taylor (1995) is a good approximation only when the pulsar systems are close to the Solar system or have a comparable distance to the Galactic centre. As shown in Fig. A1, J1713+0747 is about 1 kpc closer to the Galactic centre than the Sun. Therefore, it experiences a slightly higher vertical gravity than modelled previously in Zhu et al. (2015).

In this work, we employ a new Galactic model by McMillan (2017), which fits the rotation curve and the stellar dynamic data with an axisymmetric Galactic potential and provides a code for computing the Galactic gravitational acceleration. It is worth noting that the key input data for constraining their model regarding vertical forces were from Kuijken & Gilmore (1991) – an earlier study than Holmberg & Flynn (2004). But as shown in Fig. A1, the later Holmberg & Flynn (2004) result fits McMillan (2017) model better and the changes were relatively small. Table A1 shows J1713+0747's $\dot{P}_b^{Gal}$ computed using various Galactic potential models and the observed excess after removing Shklovskii and GR effects. One can see that most realistic models (Dehnen & Binney 1998; Binney & Tremaine 2008; Piffl et al. 2014; McMillan 2017) fit the observed excess better than the analytical approximation.

Fig. A2 shows the $\Delta \dot{P}_b^{Gal}/P_b$ using the McMillan (2017) model instead of Nice & Taylor (1995) model for a putative pulsar binary at 1 kpc distance as a function of Galactic longitude and latitude. The correction becomes of the same order of magnitudes as the observed effect $|\dot{P}_b/P_b|$ ($\sim 10^{-12}$ yr^{-1}) for J1713+0747. PSR J0437−4715 is another pulsar binary system that is sensitive to this effect (Verbiest et al. 2008; Deller et al. 2008; Reardon et al. 2016). However, at a distance of only 0.16 kpc, this pulsar's Galactic acceleration could be computed fairly accurately by Nice & Taylor (1995) model, with a $|\Delta \dot{P}_b^{Gal}/P_b| < 0.2 \times 10^{-12}$ yr^{-1}. For the other pulsar binary used in our $\dot{G}/G$ analysis – PSR J1738+0333, the correction is similar

Table A1. PSR J1713+0747's $\dot{P}_b^{Gal}$ components in units of $10^{-12}\,\mathrm{s\,s^{-1}}$, in comparison to the observed $\dot{P}_b$ where only the Shklovskii contribution has been subtracted.

Galactic potential/model	horizontal	vertical	total
McMillan (2017)	0.16	−0.50	−0.34
Piffl et al. (2014)	0.14	−0.46	−0.33
Binney & Tremaine (2008)	0.16	−0.43	−0.27
Dehnen & Binney (1998)	0.17	−0.46	−0.29
Nice & Taylor (1995)[a]	0.27	−0.36	−0.10
$\dot{P}_b^{obs} - \dot{P}_b^{Shk}$	–	–	−0.31(15)

[a]Analytical model including updates from
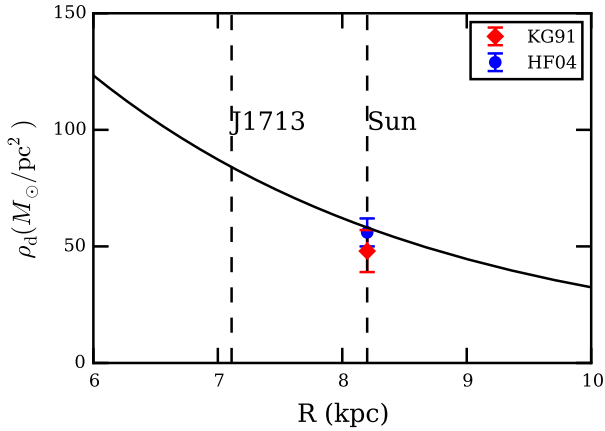Lazaridis et al. (2009), Freire et al. (2012), and Zhu et al. (2015).

Figure A1. The solid curves show the models of Galactic disc surface density as a function of Galactic radius from McMillan (2017). The error bars indicate disc surface densities from studies of the dynamics of stars in the Solar vicinity by Kuijken & Gilmore (1991) (red diamond) and Holmberg & Flynn (2004) (blue circle). The vertical lines mark the positions of the pulsar and the Sun.
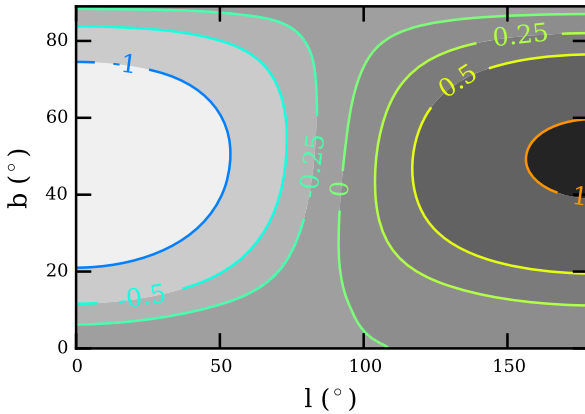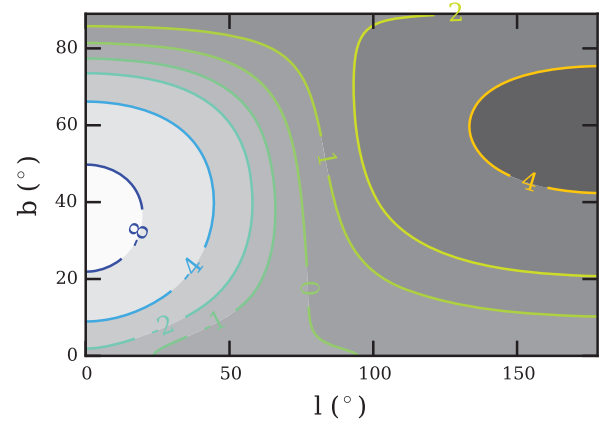

Figure A2. The difference between the Galactic corrections ($\dot{P}^{Gal}/P$ and $\dot{P}_b^{Gal}/P_b$) derived from McMillan (2017) and the Nice & Taylor (1995) approximation as a function of Galactic longitude (l) and latitude (b) for a pulsar binary at 1 kpc distance from us in units of $10^{-12}\,\mathrm{yr^{-1}}$.

to that of J1713+0747, but still relatively insignificant compared to the observational uncertainty $\delta\dot{P}_b/P_b$ of $\sim 4 \times 10^{-12}$ (Freire et al. 2012).

Since Nice & Taylor (1995) used the local disc surface density and assumed a flat rotation curve, the real Galactic potential deviates

Figure A3. The difference between the Galactic corrections ($\dot{P}^{Gal}/P$ and $\dot{P}_b^{Gal}/P_b$) derived from McMillan (2017) and the Nice & Taylor (1995) approximation as a function of Galactic longitude (l) and latitude (b) for a pulsar binary at 3 kpc distance in units of $10^{-12}\,\mathrm{yr^{-1}}$.

more from it at greater distances from the Sun. In Fig. A3, we show that at a distance of 3 kpc the extra Galactic correction $|\Delta\dot{P}_b/P_b|$ (or $|\Delta\dot{P}/P|$ for the pulsar period) comes close to $10^{-11}\,\mathrm{yr^{-1}}$ for some directions therefore a more realistic model must be used for pulsars in this situation.

Presently, there are only a handful of pulsars that are sensitive to the Galactic acceleration. In future, new telescopes such as the Five hundred meter Aperture Spherical Telescope (FAST, Nan et al. 2011; Li & Pan 2016) and the Square Kilometer Array (SKA, Kramer & Stappers 2015) could improve both the timing and distance measurement for many more pulsars such that this correction becomes significant for them. It might be possible to start using some pulsars as accelerometers for probing the Galactic gravity field and improving our knowledge of the Galactic potentials, independent to the improvements expected from *GAIA*[11] (Prusti et al. 2016) .

[1]*Max-Planck-Institut für Radioastronomie, Auf dem Hügel 69, D-53121 Bonn, Germany*
[2]*National Astronomical Observatories, Chinese Academy of Science, 20A Datun Road, Chaoyang District, Beijing 100012, China*
[3]*National Radio Astronomy Observatory, P. O. Box 0, Socorro, NM 87801, USA*
[4]*Jet Propulsion Laboratory, California Institute of Technology, 4800 Oak Grove Dr. Pasadena, CA 91109, USA*
[5]*ASTRON, the Netherlands Institute for Radio Astronomy, Postbus 2, NL-7990 AA Dwingeloo, the Netherlands*
[6]*Department of Astrophysics/IMAPP, Radboud University, PO Box 9010, NL-6500 GL Nijmegen, the Netherlands*
[7]*Jodrell Bank Centre for Astrophysics, School of Physics and Astronomy, The University of Manchester, Manchester M13 9PL, UK*
[8]*Institute of Astronomy / Battcock Centre for Astrophysics, University of Cambridge, Madingley Road, Cambridge CB3 0HA, UK*
[9]*Department of Physics, Lafayette College, Easton, PA 18042, USA*
[10]*National Radio Astronomy Observatory, Charlottesville, VA 22903, USA*
[11]*Department of Physics and Astronomy, 6224 Agricultural Road, University of British Columbia, Vancouver, BC V6T 1Z1, Canada*
[12]*Fakultät für Physik, Universität Bielefeld, Postfach 100131, D-33501 Bielefeld, Germany*
[13]*Center for Research and Exploration in Space Science and Technology and X-Ray Astrophysics Laboratory, NASA Goddard Space Flight Center, Code 662, Greenbelt, MD 20771, USA*

[11]http://sci.esa.int/gaia/

[14] *Universities Space Research Association, Columbia, MD 21046, USA*

[15] *INAF - ORA - Osservatorio Astronomico di Cagliari, via della Scienza 5, I-09047 Selargius (CA), Italy*

[16] *Laboratoire de Physique et Chimie de l'Environnement et de l'Espace LPC2E CNRS-Université d'Orléans, F-45071 Orléans, France*

[17] *Station de radioastronomie de Nançay, Observatoire de Paris, CNRS/INSU, F-18330 Nançay, France*

[18] *Department of Physics, Hillsdale College, 33 E. College Street, Hillsdale, MI 49242, USA*

[19] *Faculty of Science, University of East Anglia, Norwich Research Park, Norwich NR4 7TJ, UK*

[20] *Department of Physics, McGill University, Montreal, QC H3A 2T8, Canada*

[21] *Department of Nuclear Medicine, Vancouver Coastal Health Authority, Vancouver, BC V5Z 1M9, Canada*

[22] *Anton Pannekoek Institute for Astronomy, University of Amsterdam, Science Park 904, 1098 XH Amsterdam, the Netherlands*

[23] *Department of Physics, Columbia University, 550 W. 120th St New York, NY 10027, USA*

[24] *Department of Physics and Astronomy, West Virginia University, PO Box 6315, Morgantown, WV 26506, USA*

[25] *Center for Gravitational Waves and Cosmology, West Virginia University, Chestnut Ridge Research Building, Morgantown, WV 26505, USA*

[26] *Kavli institute for astronomy and astrophysics, Peking University, Beijing 100871, P.R. China*

[27] *Centre for Astrophysics and Supercomputing, Swinburne University of Technology, Hawthorn Vic 3122, Australia*

[28] *Hungarian Academy of Sciences MTA-ELTE Extragalactic Astrophysics Research Group, Institute of Physics, Eötvös Loránd University, Pázmáany P. s. 1/A, Budapest 1117, Hungary*

[29] *Center for Gravitation, Cosmology and Astrophysics, Department of Physics, University of Wisconsin-Milwaukee, PO Box 413, Milwaukee, WI 53201, USA*

[30] *LUTH, Observatoire de Paris, PSL Research University, CNRS, Université Paris Diderot, Sorbonne Paris Cité, F-92195 Meudon, France*

This paper has been typeset from a TEX/LATEX file prepared by the author.